AIP Journal of Applied Physics

Improvement in output power of a 460 nm InGaN light-emitting diode using staggered quantum well

Chih-Teng Liao, Miao-Chan Tsai, Bo-Ting Liou, Sheng-Horng Yen, and Yen-Kuang Kuo

Citation: Journal of Applied Physics **108**, 063107 (2010); doi: 10.1063/1.3471804
View online: http://dx.doi.org/10.1063/1.3471804
View Table of Contents: http://scitation.aip.org/content/aip/journal/jap/108/6?ver=pdfcov
Published by the AIP Publishing

Articles you may be interested in
Improvement in spontaneous emission rates for InGaN quantum wells on ternary InGaN substrate for light-emitting diodes
J. Appl. Phys. **110**, 113110 (2011); 10.1063/1.3668117

Growths of staggered InGaN quantum wells light-emitting diodes emitting at 520–525 nm employing graded growth-temperature profile
Appl. Phys. Lett. **95**, 061104 (2009); 10.1063/1.3204446

High-efficiency staggered 530 nm InGaN/InGaN/GaN quantum-well light-emitting diodes
Appl. Phys. Lett. **94**, 041109 (2009); 10.1063/1.3075853

Polarization engineering via staggered InGaN quantum wells for radiative efficiency enhancement of light emitting diodes
Appl. Phys. Lett. **91**, 091110 (2007); 10.1063/1.2775334

Carrier leakage in InGaN quantum well light-emitting diodes emitting at 480 nm
Appl. Phys. Lett. **82**, 2755 (2003); 10.1063/1.1570515

Re-register for Table of Content Alerts

Create a profile.

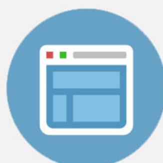

Sign up today!

[This article is copyrighted as indicated in the article. Reuse of AIP content is subject to the terms at: http://scitation.aip.org/termsconditions. Downloaded to] IP: 140.113.38.11 On: Wed, 30 Apr 2014 10:01:21

Improvement in output power of a 460 nm InGaN light-emitting diode using staggered quantum well

Chih-Teng Liao,[1] Miao-Chan Tsai,[2] Bo-Ting Liou,[3] Sheng-Horng Yen,[4] and Yen-Kuang Kuo[5,a)]
[1]*Institute of Lighting and Energy Photonics, College of Photonics, National Chiao Tung University, Tainan 711, Taiwan*
[2]*Institute of Photonics, National Changhua University of Education, Changhua 500, Taiwan*
[3]*Department of Mechanical Engineering, Hsiuping Institute of Technology, Taichung 41283, Taiwan*
[4]*R&D division, Epistar Co., Ltd., Science-based Industrial Park, Hsinchu 300, Taiwan*
[5]*Department of Physics, National Changhua University of Education, Changhua 500, Taiwan*

(Received 18 June 2010; accepted 6 July 2010; published online 24 September 2010)

Staggered quantum well structures are studied to eliminate the influence of polarization-induced electrostatic field upon the optical performance of blue InGaN light-emitting diodes (LEDs). Blue InGaN LEDs with various staggered quantum wells which vary in their indium compositions and quantum well width are theoretically studied and compared by using the APSYS simulation program. According to the simulation results, the best optical characteristic is obtained when the staggered quantum well is designed as $In_{0.20}Ga_{0.80}N$ (1.4 nm)–$In_{0.26}Ga_{0.74}N$ (1.6 nm) for blue LEDs. Superiority of this novelty design is on the strength of its enhanced overlap of electron and hole wave functions, uniform distribution of holes, and suppressed electron leakage in the LED device.
© *2010 American Institute of Physics*. [doi:10.1063/1.3471804]

I. INTRODUCTION

The visible III-nitride light-emitting diodes (LEDs) have received much attention due to their wide applications in full-color display, liquid crystal display back-lighting, mobile platforms, and illumination.[1–6] High-luminescence and high-efficiency blue InGaN LEDs, especially, are of foremost importance for application in illumination market such as outdoor display and solid-state lighting. However, several mechanisms degenerating the optical performance including light extraction efficiency, current crowding effect, high operation voltage, and piezoelectric effect remain unsolved which will sabotage the achievement of high-power blue InGaN LEDs.[7–11]

For the III-nitride system, the electrostatic field within the active region is a critical factor to poor lighting characteristic. Resulting from spontaneous and piezoelectric polarizations, the piezoelectric effect eventually leads to strong electrostatic field and band bending situation within the active region. Piezoelectric polarization is caused by stress formed in the situation when layers were grown on a lattice-mismatch substrate; spontaneous polarization results from the asymmetric structure along the [0001] axis of wurtzite structures.[12–14] The large electrostatic field within the active region results in quantum confined Stark effect and poor overlap of electron and hole wave functions, and it consequently reduces the radiative recombination rate and internal quantum efficiency of the optoelectronic devices. To minimize the piezoelectric effect of blue InGaN LEDs, several specific structure designs such as heavily Si-doping in quantum barriers,[15–17] nonpolar (*a*- and *m*-planes) quantum wells (QWs) grown on *r*-plane sapphire and γ-$LiAlO_2$,[18–22] semipolar QWs grown on *m*-plane sapphire,[23–27] polarization-matched AlGaInN layers,[28,29] and staggered-QW structures have been proposed.[30–39] For InGaN LEDs, as the overlap of electron and hole wave functions improves, the photoluminescence lifetime will decrease, and the radiative recombination rate and optical gain will be accordingly enhanced; hence, the percentage of carrier leakage would be reduced owing to carriers that effectively contribute toward radiative recombination. In addition, although the above-mentioned methods are useful for abating the piezoelectric effect, staggered-InGaN QW LEDs have the merit of an identical growth process to the conventional structures that makes commercial fabrication possible and substantial. After the concept of the staggered-InGaN-QW structure was proposed by Arif *et al.*[30] for the first time, various similar designs including type-II InGaN QW,[40–42] strain-compensated InGaN-AlGaN QW,[43,44] three-layer staggered-InGaN QW,[35,36,39] InGaN QW with AlGaN δ-layer,[45–47] and dip-shaped InGaN/GaN QW (Ref. 37) have been recommended to decrease the strong polarization-induced electrostatic field in the GaN-based optoelectronic devices. Therefore, the focus of the current research is upon staggered-QW LEDs; by adjusting the indium composition and well width of the staggered QWs, the authors seek to accomplish better optical performance of blue InGaN LEDs.

In this work, various staggered-InGaN QW LEDs are theoretically studied in detail by using the APSYS (abbreviation of advanced physical models of semiconductor devices)[48] simulation program. By performing computational simulations, the authors examine proper designs of staggered-QW blue LEDs and the critical physical mechanisms behind the improvement of the optical performance.

[a)]Electronic mail: ykuo@cc.ncue.edu.tw.

 © 2010 American Institute of Physics

[This article is copyrighted as indicated in the article. Reuse of AIP content is subject to the terms at: http://scitation.aip.org/termsconditions. Downloaded to] IP: 140.113.38.11 On: Wed, 30 Apr 2014 10:01:21

TABLE I. Band gap energy of GaN, AlN, and InN.

	Alloy		
Parameter	GaN	AlN	InN
$E_g(0)$ (eV)	3.507	6.23	0.735
α (meV/K)	0.909	1.799	0.245
β (K)	830	1462	624

II. SIMULATION PARAMETERS AND DEVICE STRUCTURE

The band gap energies of GaN, AlN, InN, and other binary alloys at temperature T can be expressed by the Varshni formula[49]

$$E_g(T) = E_g(0) - \frac{\alpha \cdot T^2}{T + \beta}, \tag{1}$$

where $E_g(T)$ is the band gap energy at temperature T, $E_g(0)$ is the band gap energy at 0 K, α and β are material-related constants. Table I lists the band gap energies of GaN, AlN, and InN used in our simlulation.[49,50] Besides, for $In_xGa_{1-x}N$ and $Al_xGa_{1-x}N$ ternary alloys, the band gap energies can be described as a linear combination of GaN, AlN, or InN binary alloys and a second-order correction as the following formula:[51]

$$E_g(In_xGa_{1-x}N) = E_{g,InN} \cdot x + E_{g,GaN} \cdot (1-x) - b \cdot x \cdot (1-x), \tag{2}$$

$$E_g(Al_xGa_{1-x}N) = E_{g,AlN} \cdot x + E_{g,GaN} \cdot (1-x) - b \cdot x \cdot (1-x), \tag{3}$$

where $E_g(In_xGa_{1-x}N)$ and $E_g(Al_xGa_{1-x}N)$ are the band gap energies of $In_xGa_{1-x}N$ and $Al_xGa_{1-x}N$, and the band gap bowing parameters, b, of $In_xGa_{1-x}N$ and $Al_xGa_{1-x}N$ are adopted to be 2.8 eV and 0.7 eV, respectively.[52] Other material parameters of the relevant binary semiconductors used in the simulation can be found in Ref. 52.

In addition, it is important to take into consideration the built-in polarization induced by spontaneous and piezoelectric polarizations at heterointerfaces of nitride related devices since it plays an essential role for III-nitride optical devices. To calculate the built-in polarization induced by spontaneous and piezoelectric polarizations at heterointerfaces of III-nitride LEDs, the method developed by Bernardini[12] is employed to estimate the fixed interface charges. The spontaneous polarization of ternary nitride alloys can be expressed by the formulas with bowing terms as shown in Eqs. (4) and (5)

$$P_{sp}(Al_xGa_{1-x}N) = x \cdot P_{sp}(AlN) + (1-x) \cdot P_{sp}(GaN) + B(AlGaN) \cdot x \cdot (1-x), \tag{4}$$

$$P_{sp}(In_xGa_{1-x}N) = x \cdot P_{sp}(InN) + (1-x) \cdot P_{sp}(GaN) + B(InGaN) \cdot x \cdot (1-x), \tag{5}$$

where $P_{sp}(InN)$, $P_{sp}(AlN)$, and $P_{sp}(GaN)$ are values of spontaneous polarization of InN, AlN, and GaN alloys, which are set to be $-0.042\ C/m^2$, $-0.090\ C/m^2$, and $-0.034\ C/m^2$, respectively; $B(InGaN)$ and $B(AlGaN)$ are spontaneous polarization bowing parameters of InGaN and AlGaN, which are $-0.037\ C/m^2$ and $-0.021\ C/m^2$, respectively.[52]

On the other hand, the piezoelectric polarization of AlGaN and InGaN can be calculated by the following formulas:

$$P_{pz}(Al_xGa_{1-x}N) = P_{pz}(AlN) \cdot x + P_{pz}(GaN) \cdot (1-x), \tag{6}$$

$$P_{pz}(In_xGa_{1-x}N) = P_{pz}(InN) \cdot x + P_{pz}(GaN) \cdot (1-x), \tag{7}$$

where

$$P_{pz}(AlN) = -1.808 \cdot \varepsilon + 5.624 \cdot \varepsilon^2 \quad \text{for } \varepsilon < 0, \tag{8}$$

$$P_{pz}(AlN) = -1.808 \cdot \varepsilon - 7.888 \cdot \varepsilon^2 \quad \text{for } \varepsilon > 0, \tag{9}$$

$$P_{pz}(GaN) = -0.918 \cdot \varepsilon + 9.541 \cdot \varepsilon^2, \tag{10}$$

$$P_{pz}(InN) = -1.373 \cdot \varepsilon + 7.559 \cdot \varepsilon^2. \tag{11}$$

The basal strain matched to a GaN layer for the alloy in this study is defined as

$$\varepsilon = (a_{sub} - a)/a, \tag{12}$$

where a_{sub} and a are the lattice constants of GaN and alloy layers, respectively. Total polarization is obtained by summing the values of spontaneous and piezoelectric polarizations. Note that the amount of surface charges obtained from the experimental measurement is usually smaller than those obtained by theoretical calculation. The surface charges could be screened due to the defects inside the device and the screening percentage commonly ranges between 20% and 80% for InGaN materials.[53,54] To ascertain identical results of the simulated data to the original structure, approach real situation, 40% of the calculated surface charge density is assumed in our simulation.

The simulated InGaN blue LED used as a reference for subsequent analysis is based on the structure fabricated by Chang *et al.*[55] The device geometry was a rectangular shape design with dimensions of $400 \times 320\ \mu m^2$. This LED was grown on a c-plane sapphire substrate, followed by a GaN buffer layer. A 3 μm thick Si-doped n-GaN layer with a doping concentration of $1 \times 10^{18}\ cm^{-3}$ was used to be the n-type contact layer. The active region consisted of five 3 nm thick $In_{0.23}Ga_{0.77}N$ QWs separated by six 7 nm thick GaN barriers. On top of the active region was a 50 nm thick Mg-doped p-$Al_{0.15}Ga_{0.85}N$ electron-blocking layer (EBL) with a doping concentration of $3 \times 10^{17}\ cm^{-3}$. A 0.25 μm thick Mg-doped p-GaN contact layer with a doping concentration of $5 \times 10^{17}\ cm^{-3}$ was grown to complete the structure.

To simplify the structure referred, the number of QW in our simulation is remained to be one. Therefore, the subsequent investigations are for the blue InGaN LED with single QW (SQW) and the schematic diagram could be referred in Fig. 1. To model the staggered-QW structure, the original $In_{0.23}Ga_{0.77}N$ QW layer is divided into two layers, which are layer I close to the n-layers and layer II close to the p-layers; the schematic diagram of the staggered-QW is presented in Fig. 2. Note that the total thickness of the InGaN QW is fixed for all the structures considered in the subsequent discussion.

[This article is copyrighted as indicated in the article. Reuse of AIP content is subject to the terms at: http://scitation.aip.org/termsconditions. Downloaded to] IP: 140.113.38.11 On: Wed, 30 Apr 2014 10:01:21

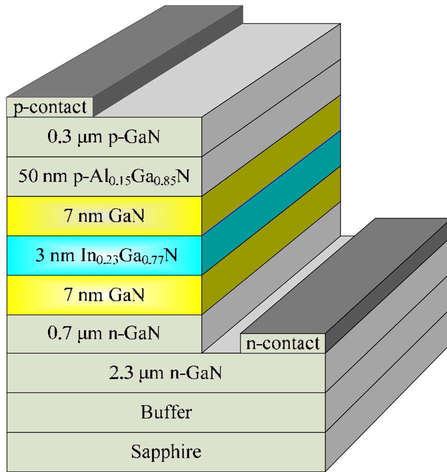

FIG. 1. (Color online) Schematic diagram of the SQW LED in this study.

Steps in exploring the most appropriate design of layers I and II in the simulation are illustrated as the following. First, the indium composition of layer I increased from 0.20 to 0.26 while that of layer II decreased from 0.26 to 0.20, correspondingly. Then, the width of layer I changed from 0.5 to 2.5 nm and that of layer II changed from 2.5 nm to 0.5 nm accordingly. Figure 3 shows the output power and emission wavelength of each staggered-QW LED of which the indium composition for each structure ranges from 0.20 to 0.26 and well width ranges from 0.5 to 2.5 nm. Based on Fig. 3, the authors enumerated a few appropriate staggered-QW designs which sustained the InGaN LEDs emitting at approximately 460 nm and, at the same time, enhanced the lighting power of the devices. After comparing, preferable designs of the staggered QWs are $In_{0.20}Ga_{0.80}N$ (1.4 nm)–$In_{0.26}Ga_{0.74}N$ (1.6 nm), $In_{0.21}Ga_{0.79}N$ (1.4 nm)–$In_{0.25}Ga_{0.75}N$ (1.6 nm), and $In_{0.22}Ga_{0.78}N$ (1.5 nm)–$In_{0.24}Ga_{0.76}N$ (1.5 nm), which are named as structure A, structure B, and structure C, respectively.

III. SIMULATION RESULTS AND DISCUSSION

The simulated light-current-voltage (L-I-V) performance curves of structure A, B, and C, as well as the original one are plotted in Fig. 4. From Fig. 4, it is apparent that all the three staggered-QW LEDs possess better lighting characteristic than the original one while the electrical performances of these devices are similar. To scrutinize the main physical factors to the improvement in the lighting performance of staggered-QW LEDs, optical characteristics of structure A possessing the best performance and the original structure, including band diagram, overlap between electron and hole

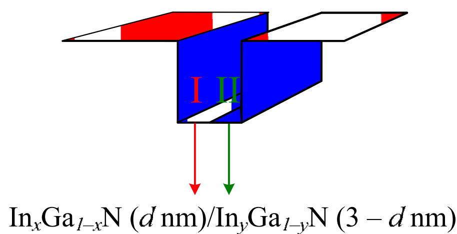

FIG. 2. (Color online) Schematic diagram of the staggered-QW.

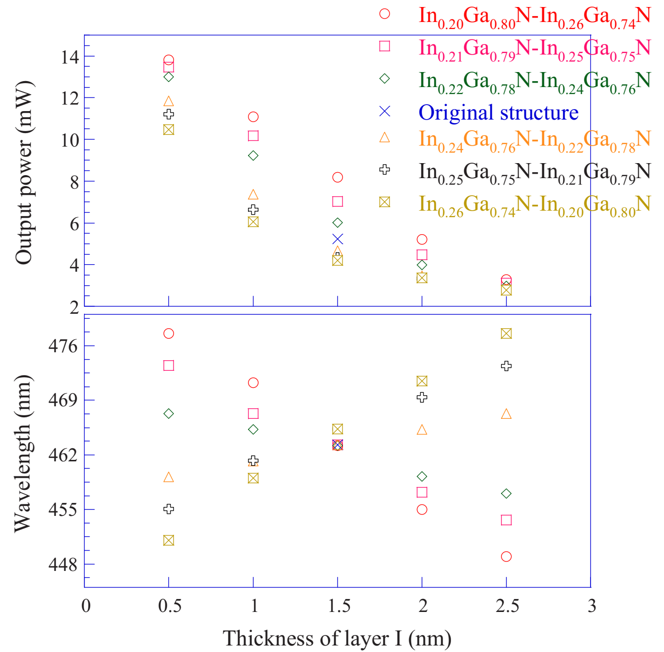

FIG. 3. (Color online) Output power and emission wavelength of varied staggered-QW LEDs.

wave functions in the QW, electrostatic field, and carrier distribution, are compared and discussed in the following paragraph.

First, the emission spectra of structure A and the original structure are plotted in Fig. 5. The emitting spectra are peaked at around 460 nm and furthermore the spontaneous emission rate of structure A is effectively enhanced as compared with the original structure. In Fig. 6, the band diagrams with ground-state electron and hole wave functions of structure A and the original structure at 20 mA are presented. It could be found that for structure A which features a design of InGaN QW, the tilted valence band within the QW is reformed because of the step-like shape. In another word, structure A has the merit of more uniform distribution of holes inside the QW when compared with the original structure. As a result of right-shifted hole wave function, the overlap of electron and hole wave functions in structure A is improved. The percentage of overlap between electron and hole wave functions is 14.9% for structure A and 13.9% for the original structure.

Second, the electron concentration and conduction band

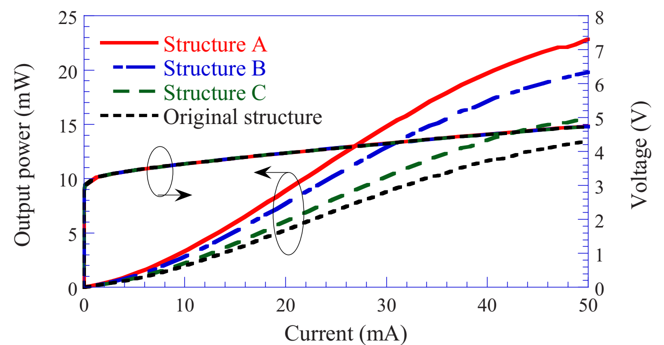

FIG. 4. (Color online) Simulated L-I-V curves of structure A, B, C, and original structure.

[This article is copyrighted as indicated in the article. Reuse of AIP content is subject to the terms at: http://scitation.aip.org/termsconditions. Downloaded to] IP: 140.113.38.11 On: Wed, 30 Apr 2014 10:01:21

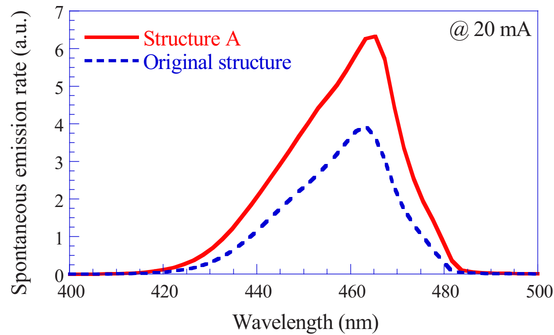

FIG. 5. (Color online) Emission spectra of structure A and original structure at 20 mA.

in the active region for structure A and the original structure at 20 mA are shown in Fig. 7(a) while the hole concentration and valence band for them are presented in Fig. 7(b). The gray areas in the figures represent the locations of the QW. For ordinary blue InGaN LEDs, since holes are the minority carriers in the active region, the radiative emission is dominated mainly by holes. It can be easily observed that hole distribution within the QW for structure A is right-shifted due to little sagged valence band as shown in Fig. 7(b). Moreover, the negative electrostatic field within the active region of structure A is larger than that of the original structure as indicated in Fig. 8. Figure 9 schematically presents the polarization charges at each interface within the active region for structure A and the original structure. The strengthened negative electrostatic field of structure A results from the larger lattice-mismatch between the $In_{0.26}Ga_{0.74}N$ well layer and the GaN barrier layer as compared with the difference between the $In_{0.23}Ga_{0.77}N$ well layer and the GaN barrier layer in the original structure as shown in Fig. 9. Since a large negative electrostatic field contributes to hole injection into the QW, consequently, it is anticipated that,

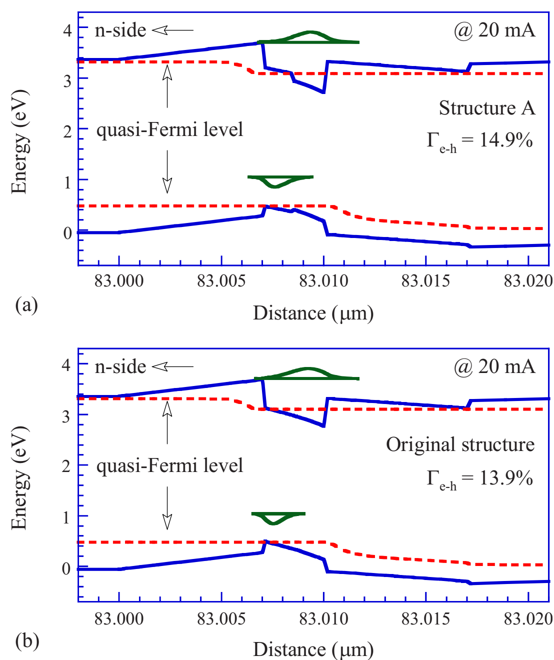

FIG. 6. (Color online) Band diagrams with ground-state electron and hole wave functions of (a) structure A and (b) original structure at 20 mA.

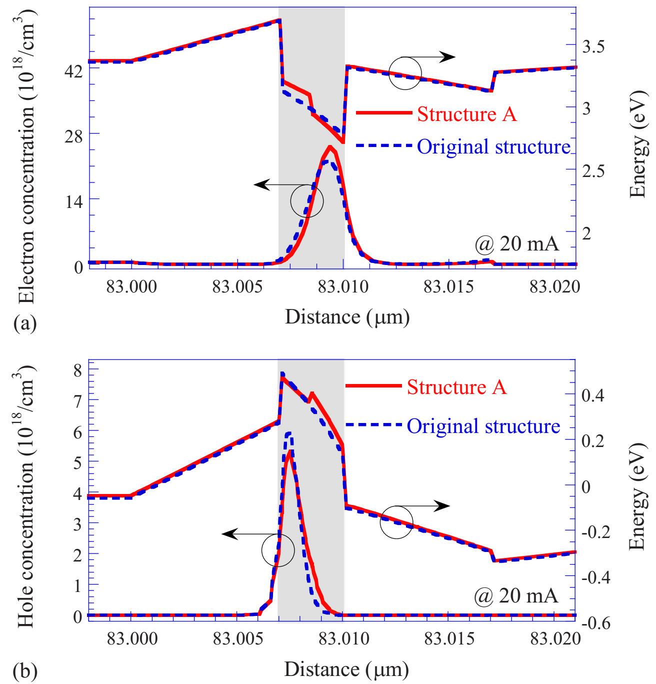

FIG. 7. (Color online) (a) Electron concentration together with conduction band diagram and (b) hole concentration together with valence band diagram for structure A and original structure at 20 mA.

compared with the original structure, structure A may possess more holes inside the QW. When comparing the area under the curves of hole concentration for these two structures, we conclude an increase of 1% of the hole concentration inside the QW in structure A. Given that right-shifted hole distribution and larger amounts of holes inside the QW lead to improvement in overlap of electrons and holes, the recombination of electrons and holes is enhanced, and the emission power is increased correspondingly in structure A.

Third, Fig. 10 indicates the conduction band diagrams of structure A and the original structure at 20 mA. After calculating, the effective potential heights of structure A and the original structure (which are the difference between the conduction band energy of the EBL and quasi-Fermi level) are 201 meV and 173 meV, respectively. Due to larger effective potential height, structure A has a smaller percentage of electron leakage of 6.5% when compared with the original structure (11.9%). In other words, larger amounts of holes inside the QW as well as increased overlap of electron and hole

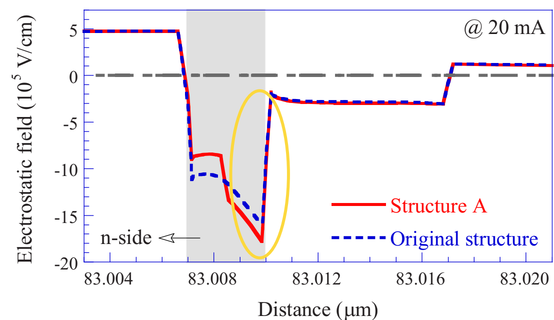

FIG. 8. (Color online) Built-in electrostatic field within the active region of structure A and original structure at 20 mA.

[This article is copyrighted as indicated in the article. Reuse of AIP content is subject to the terms at: http://scitation.aip.org/termsconditions. Downloaded to] IP: 140.113.38.11 On: Wed, 30 Apr 2014 10:01:21

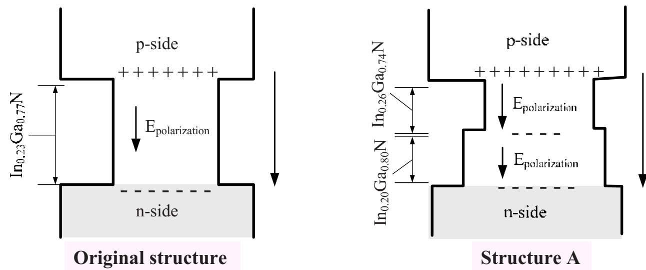

FIG. 9. (Color online) Schematic diagram of polarization charges at each interface within the active region for structure A and original structure.

wave functions result in more electrons contributing to radiative recombination. Therefore, the issue of electron leakage, accordingly, is diminished.

Finally, considering the Shockley–Read–Hall (SRH) recombination rate of structure A and the original structure at 20 mA (see Fig. 11), the authors integrated areas under the curves of SRH recombination rates for the two structures and found that structure A possessed less SRH recombination, which is the effect of nonradiative recombination. Therefore, for structure A, owing to an increase in overlap of electron and hole wave functions, there will be less carriers inside the QW recombining via nonradiative recombination process and more carriers through radiative recombination process when compared with the original structure.

IV. CONCLUSION

Optical characteristics of various staggered-InGaN-QW LEDs, which are designed to debase the significant piezoelectric effect of blue InGaN LEDs, are numerically investigated in this study by using the APSYS simulation program. Indium composition and width of the staggered-QW are adjusted to obtain the optimal structure and the corresponding optical performance including emission wavelength, band diagram, and carrier distribution are investigated and compared. According to the simulation results, predicaments such as overlap of electron and hole wave functions, inhomogeneous carrier distribution inside the QW, electron leakage, and SRH recombination rate in the active region are remarkably improved in the $In_{0.20}Ga_{0.80}N$ (1.4 nm)–$In_{0.26}Ga_{0.74}N$ (1.6 nm) staggered-QW structure. Therefore, it is concluded that the best optical performance is obtained in the blue InGaN LED characterized by the design of an $In_{0.20}Ga_{0.80}N$ (1.4 nm)–$In_{0.26}Ga_{0.74}N$ (1.6 nm) QW.

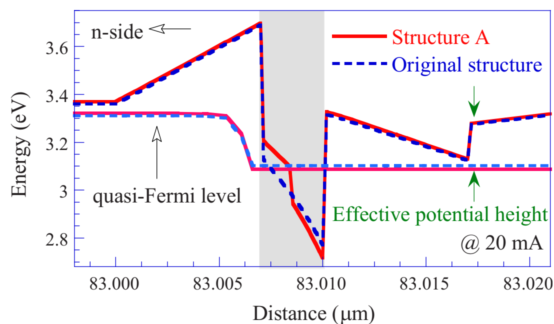

FIG. 10. (Color online) Conduction band diagrams of structure A and original structure at 20 mA.

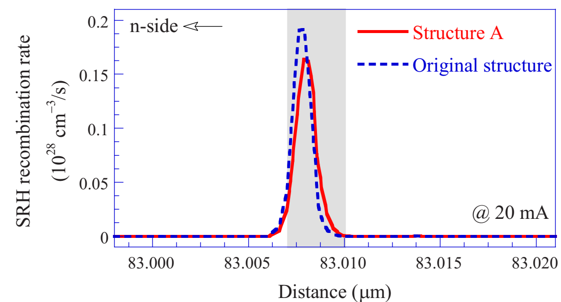

FIG. 11. (Color online) SRH recombination rate of structure A and original structure at 20 mA.

ACKNOWLEDGMENTS

This work is supported by the National Science Council (NSC) of Taiwan under Grant No. NSC 96-2112-M-018-007-MY3. The authors are grateful to Crosslight Software Inc., Canada, for the development of the APSYS simulation program used in this study and Dr. Jen-De Chen for the technical assistance.

[1]J. Shakya, K. Knabe, K. H. Kim, J. Li, J. Y. Lin, and H. X. Jiang, Appl. Phys. Lett. **86**, 091107 (2005).
[2]J. Li, J. Y. Lin, and H. X. Jiang, Appl. Phys. Lett. **88**, 171909 (2006).
[3]Y. A. Chang, C. Y. Luo, H. C. Kuo, Y. K. Kuo, C. F. Lin, and S. C. Wang, Jpn. J. Appl. Phys., Part 1 **44**, 7916 (2005).
[4]P. T. Barletta, E. A. Berkman, B. F. Moody, N. A. El-Masry, A. M. Emara, M. J. Reed, and S. M. Bedair, Appl. Phys. Lett. **90**, 151109 (2007).
[5]K. S. Kim, J. H. Kim, S. J. Jung, Y. J. Park, and S. N. Cho, Appl. Phys. Lett. **96**, 091104 (2010).
[6]S. Choi, H. J. Kim, S.-S. Kim, J. Liu, J. Kim, J.-H. Ryou, R. D. Dupuis, A. M. Fischer, and F. A. Ponce, Appl. Phys. Lett. **96**, 221105 (2010).
[7]C. H. Kuo, S. J. Chang, Y. K. Su, L. W. Wu, J. F. Chen, J. K. Sheu, and J. M. Tsai, IEEE Trans. Electron Devices **50**, 535 (2003).
[8]Y. K. Su, S. J. Chang, S. C. Wei, R. W. Chuang, S. M. Chen, and W. L. Li, IEEE Electron Device Lett. **26**, 891 (2005).
[9]C. F. Shen, S. J. Chang, W. S. Chen, T. K. Ko, C. T. Kuo, and S. C. Shei, IEEE Photonics Technol. Lett. **19**, 780 (2007).
[10]T. Onuma, H. Amaike, M. Kubota, K. Okamoto, H. Ohta, J. Ichihara, H. Takasu, and S. F. Chichibu, Appl. Phys. Lett. **91**, 181903 (2007).
[11]C. E. Lee, H. C. Kuo, Y. C. Lee, M. R. Tsai, T. C. Lu, S. C. Wang, and C. T. Kuo, IEEE Photonics Technol. Lett. **20**, 184 (2008).
[12]F. Bernardini, in *Nitride Semiconductor Devices: Principles and Simulation*, edited by J. Piprek (Wiley, New York, 2007), p. 4968.
[13]A. Thamm, O. Brandt, J. Ringling, A. Trampert, and K. H. Ploog, Phys. Rev. B **61**, 16025 (2000).
[14]A. E. Romanov, T. J. Baker, S. Nakamura, and J. S. Speck, J. Appl. Phys. **100**, 023522 (2006).
[15]Y.-H. Cho, J. J. Song, S. Keller, M. S. Minsky, E. Hu, U. K. Mishra, and S. P. DenBaars, Appl. Phys. Lett. **73**, 1128 (1998).
[16]E. Oh, C. Sone, O. Nam, H. Park, and Y. Park, Appl. Phys. Lett. **76**, 3242 (2000).
[17]G. Franssen, T. Suski, P. Perlin, R. Bohdan, A. Bercha, W. Trzeciakowski, I. Makarowa, P. Prystawko, M. Leszczyński, I. Grzegory, S. Porowski, and S. Kokenyesi, Appl. Phys. Lett. **87**, 041109 (2005).
[18]P. Waltereit, O. Brandt, A. Trampert, H. T. Grahn, J. Menniger, M. Ramsteiner, M. Reiche, and K. H. Ploog, Nature (London) **406**, 865 (2000).
[19]A. Chakraborty, B. A. Haskell, S. Keller, J. S. Speck, S. P. DenBaars, S. Nakamura, and U. K. Mishra, Appl. Phys. Lett. **85**, 5143 (2004).
[20]R. Kröger, T. Paskova, S. Figge, D. Hommel, A. Rosenauer, and B. Monemar, Appl. Phys. Lett. **90**, 081918 (2007).
[21]A. Kobayashi, S. Kawano, K. Ueno, J. Ohta, H. Fujioka, H. Amanai, S. Nagao, and H. Horie, Appl. Phys. Lett. **91**, 191905 (2007).
[22]T. Paskova, Phys. Status Solidi **245**, 1011 (2008) (b).
[23]A. Chakraborty, T. J. Baker, B. A. Haskell, F. Wu, J. S. Speck, S. P. DenBaars, S. Nakamura, and U. K. Mishra, Jpn. J. Appl. Phys., Part 1 **44**, L945 (2005).
[24]R. Sharma, P. M. Pattison, H. Masui, R. M. Farrell, T. J. Baker, B. A.

[This article is copyrighted as indicated in the article. Reuse of AIP content is subject to the terms at: http://scitation.aip.org/termsconditions. Downloaded to] IP: 140.113.38.11 On: Wed, 30 Apr 2014 10:01:21

Haskell, F. Wu, S. P. DenBaars, J. S. Speck, and S. Nakamura, Appl. Phys. Lett. **87**, 231110 (2005).
[25]M. Ueda, K. Kojima, M. Funato, Y. Kawakami, Y. Narukawa, and T. Mukai, Appl. Phys. Lett. **89**, 211907 (2006).
[26]K. Kojima, M. Funato, Y. Kawakami, S. Masui, S. Nagahama, and T. Mukai, Appl. Phys. Lett. **91**, 251107 (2007).
[27]P. Vennéguès, Z. Bougrioua, and T. Gunehne, Jpn. J. Appl. Phys., Part 1 **46**, 4089 (2007).
[28]M.-H. Kim, M. F. Schubert, Q. Dai, J. K. Kim, E. F. Schubert, J. Piprek, and Y. Park, Appl. Phys. Lett. **91**, 183507 (2007).
[29]M. F. Schubert, J. Xu, J. K. Kim, E. F. Schubert, M. H. Kim, S. Yoon, S. M. Lee, C. Sone, T. Sakong, and Y. Park, Appl. Phys. Lett. **93**, 041102 (2008).
[30]R. A. Arif, Y.-K. Ee, and N. Tansu, Appl. Phys. Lett. **91**, 091110 (2007).
[31]R. A. Arif, H. Zhao, Y.-K. Ee, and N. Tansu, IEEE J. Quantum Electron. **44**, 573 (2008).
[32]S.-H. Yen and Y.-K. Kuo, Opt. Commun. **281**, 4735 (2008).
[33]S.-H. Park, D. Ahn, B.-H. Koo, and J.-W. Kim, Phys. Status Solidi A **206**, 2637 (2009).
[34]H. Zhao, R. A. Arif, and N. Tansu, IEEE J. Sel. Top. Quantum Electron. **15**, 1104 (2009).
[35]H. Zhao, G. Liu, X.-H. Li, G. S. Huang, J. D. Poplawsky, S. T. Penn, V. Dierolf, and N. Tansu, Appl. Phys. Lett. **95**, 061104 (2009).
[36]H. P. Zhao, G. Y. Liu, X. H. Li, R. A. Arif, G. S. Huang, J. D. Poplawsky, S. T. Penn, V. Dierolf, and N. Tansu, IET Optoelectron. **3**, 283 (2009).
[37]S.-H. Park, D. Ahn, B.-H. Koo, and J.-W. Kim, Appl. Phys. Lett. **95**, 063507 (2009).
[38]S.-H. Park, D. Ahn, and J.-W. Kim, Appl. Phys. Lett. **94**, 041109 (2009).
[39]H. Zhao and N. Tansu, J. Appl. Phys. **107**, 113110 (2010).
[40]R. A. Arif, H. Zhao, and N. Tansu, Appl. Phys. Lett. **92**, 011104 (2008).
[41]H. Zhao, R. A. Arif, and N. Tansu, J. Appl. Phys. **104**, 043104 (2008).
[42]S.-H. Park, D. Ahn, B.-H. Koo, and J.-E. Oh, Appl. Phys. Lett. **96**, 051106 (2010).
[43]H. Zhao, R. A. Arif, Y.-K. Ee, and N. Tansu, Opt. Quantum Electron. **40**, 301 (2008).
[44]H. Zhao, R. A. Arif, Y.-K. Ee, and N. Tansu, IEEE J. Quantum Electron. **45**, 66 (2009).
[45]J. Park and Y. Kawakami, Appl. Phys. Lett. **88**, 202107 (2006).
[46]J. Park, A. Kaneta, M. Funato, and Y. Kawakami, IEEE J. Quantum Electron. **42**, 1023 (2006).
[47]S.-H. Park, J. Park, and E. Yoon, Appl. Phys. Lett. **90**, 023508 (2007).
[48]APSYS by Crosslight Software Inc., Burnaby, Canada, http://www.crosslight.com
[49]I. Vurgaftman, J. R. Meyer, and L. R. Ram-Mohan, J. Appl. Phys. **89**, 5815 (2001).
[50]T. Matsuoka, H. Okamoto, M. Nakao, H. Harima, and E. Kurimoto, Appl. Phys. Lett. **81**, 1246 (2002).
[51]G. B. Stringfellow and M. G. Craford, *High Brightness Light Emitting Diodes* (Academic, San Diego, 1997).
[52]I. Vurgaftman and J. R. Meyer, J. Appl. Phys. **94**, 3675 (2003).
[53]H. Zhang, E. J. Miller, E. T. Yu, C. Poblenz, and J. S. Speck, Appl. Phys. Lett. **84**, 4644 (2004).
[54]F. Renner, P. Kiesel, G. H. Döhler, M. Kneissl, C. G. Van de Walle, and N. M. Johnson, Appl. Phys. Lett. **81**, 490 (2002).
[55]S. J. Chang, C. S. Chang, Y. K. Su, C. T. Lee, W. S. Chen, C. F. Shen, Y. P. Hsu, S. C. Shei, and H. M. Lo, IEEE Trans. Adv. Packag. **28**, 273 (2005).

[This article is copyrighted as indicated in the article. Reuse of AIP content is subject to the terms at: http://scitation.aip.org/termsconditions. Downloaded to] IP: 140.113.38.11 On: Wed, 30 Apr 2014 10:01:21